Front. Phys. 12(5), 128103 (2017)
DOI 10.1007/s11467-017-0708-4

RESEARCH ARTICLE

Minority carrier lifetime evaluation of periphery edge region in high-performance multicrystalline ingot produced by seed-assisted directional solidification

Zhong Li[1], **Jia-Dan Li**[2], **Lin Zhuang**[2], **Rui-Jiang Hong**[2,†]

[1] *College of Physics and Electronic Information Engineering, Qinghai Nationalities University, Xining 810007, China*
[2] *Guangdong Provincial Key Laboratory of Photovoltaic Technology, School of Physics, Sun Yat-sen University, Guangzhou 510006, China*
Corresponding author. E-mail: †*hongruij@mail.sysu.edu.cn*
Received March 21, 2017; accepted June 29, 2017

A high-performance multicrystalline silicon (mc-Si) ingot was produced by seed-assisted directional solidification, and the minority carrier lifetime of the periphery edge region was evaluated. The defects and impurities in the periphery edge region of the silicon wafers were systematically studied with photoluminescence (PL) imaging, minority carrier lifetime mapping, and Fourier transform infrared (FTIR) spectroscopy. Their relationships with the minority carrier lifetime were investigated. The concentration of substitutional carbon, interstitial oxygen, and dislocation clusters is not directly correlated with the low minority carrier lifetime of the edge zone of the mc-Si ingot. Inhomogeneous grain size distribution and contamination with iron impurities were demonstrated to be the main factors affecting the low minority carrier lifetime. By controlling the impurities and improving the grain size distribution, a modified furnace was designed and a higher-quality mc-Si ingot was manufactured.

Keywords minority carrier lifetime, periphery edge, seed-assisted directional solidification, defects, impurity

PACS numbers 81.10.Fq, 81.05.Ea

Frontiers of Physics

1 Introduction

Multicrystalline silicon (mc-Si) is one of the most important materials of solar cells in the photovoltaic industry [1–5]. During directional solidification (DS) of a common mc-Si ingot, many defects and impurities can be generated, which are harmful to the solar cell performance. Therefore, the conversion efficiency of a solar cell (mc-Si) is usually lower than that of cells fabricated with monocrystalline silicon. Currently, seed-assisted crystalline silicon growth technology is being developed. The mc-silicon seed is placed in the bottom of the crucible to provide numerous fine nucleation points for the controlled grain growth. Based on this technology, a high-performance ingot with uniform grain size and low amounts of dislocations is obtained [6–8]. A higher average solar cell conversion efficiency of ∼0.5%–1% is achieved using high-performance mc-silicon compared with that of common mc-silicon based on the same cell fabrication process. The minority carrier lifetime is a crucial parameter indicating the quality of a mc-Si ingot. Localized low-lifetime regions (red zone) are frequently found at the top, bottom, and periphery edges. Many studies proved that Fe impurities of the crucible are crucial factors affecting the low-lifetime edge of mc-Si quality [9–13].

On the other hand, during the production of industrial mc-Si ingots with and without seeds, the furnace structure, temperature distribution, and solidification process significantly differ. Therefore, it is very difficult to use the same industrial furnace to manufacture and compare two mc-Si ingots with and without seeds. Another method was used to confirm the effect of the seed region on the low lifetime of the periphery edge of a high-performance mc-Si ingot. The seed preservation of the

© Higher Education Press and Springer-Verlag Berlin Heidelberg 2017

side brick (S-brick) and central brick (C-brick) of the ingot is completely different; only the S-brick is in contact with the side and bottom crucible. Therefore, S-brick and C-brick cut from the same ingot were chosen to investigate the effect of the side crucible and seed preservation on the low lifetime of the periphery edge. Possible factors limiting the lifetime of high-performance mc-Si include impurities and structural defects [14]. However, few studies reported the effect of seed preservation on the lifetime distribution, especially the lifetime of the periphery edge region.

In this paper, defects, including dislocations and grain boundaries, were studied by photoluminescence (PL) imaging. Iron impurities were detected using the SEMILAB WT-2000 instrument and a microwave photoconductivity decay technique (μ-PCD); the key of this technique is lifetime measurement before and after breaking Fe-B pairs [15]. Impurities, including substitutional carbon and interstitial oxygen, were also investigated with Fourier transform infrared (FTIR) spectroscopy. In addition, modifications were discussed and applied to improve the ingot quality.

2 Experimental

The experiment was carried out using a seed-assisted directional solidification process to cast the high-performance mc-Si ingot in an optimized directional solidification furnace (GT Advanced Technologies, GT-DSS 450HP). Each ingot was cut into 25 bricks (Fig. 1, left), A13 was chosen as C-brick and B11 was selected as S-brick for minority carrier lifetime (SEMILAB WT-2000) and infrared (SEMILAB IRB50) analyses (Fig. 1, right). The height of the C- and S-brick was 330 mm. The bottom and top ends of the two bricks were cut at 55 mm and 30 mm, respectively, to cut off lower lifetime regions. Square-shaped wafers were cut from the top, middle, and bottom parts of the two bricks (after cutting off the bottom and top ends). The wafer samples were cleaned in a standard RCA sequence and then measured with the PL imaging instrument (BT imaging, LIS-R1). From the bottom silicon wafers of the two bricks with typical low-lifetime periphery edge, 20 mm × 20 mm square silicon chips were cut perpendicular to the low-lifetime edge with a laser. The silicon chip samples were used for impurity analysis; the detailed process was reported in our preliminary work [15].

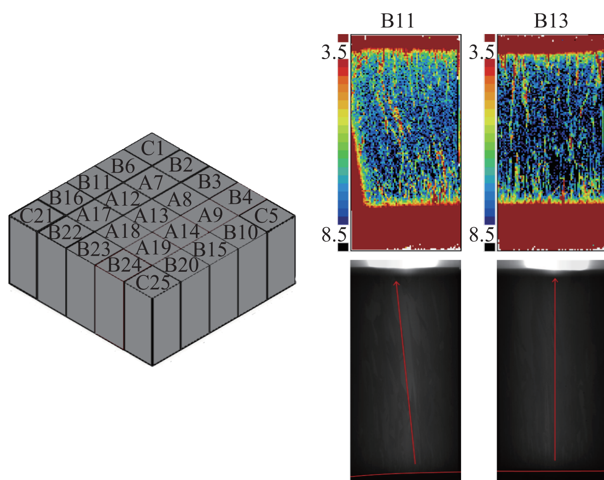

Fig. 1 Numbering of bricks of mc-Si ingot (left) and maps of the minority carrier lifetime and IR spectra of the central brick (A13) and side brick (B11, right).

3 Results and discussion

3.1 Minority carrier lifetime distribution and seed preservation

The result of the lifetime and infrared measurements are presented in Fig. 1. In addition to low minority carrier lifetimes at the top and bottom edges of the two bricks, localized low lifetime of the periphery edge was only detected in the S-brick. The periphery edge indicates that the low-lifetime region of the S-brick is larger than that of the C-brick. The lifetime measurement results in Fig. 2 also confirm that the average lifetime of the S-brick is lower than that of the C-brick. The lifetime distribution of the C-brick is homogeneous in the range from 100 mm to 250 mm and the average lifetime of the C-brick is ∼ 5.69 μs based on the μ-PCD measurement, which is larger than that of the S-brick (5.37 μs). With respect to the infrared measurement results in Fig. 1, the black area below the red lines corresponds to the preserved seed crystal region. Notably, the surface of the seed region of the C-brick is flatter than that of the S-brick. Based on the comparison of the red arrows, the columnar crystals of the C-brick grew vertically, different from that of the S-brick.

3.2 Defects

Figure 3 shows the PL maps of the silicon wafers obtained at different positions of the S-brick and C-brick. The purple region in the PL map corresponds to the area with dislocation clusters, while the green line and brown regions represent the grain boundaries and low-lifetime regions, respectively. The purple regions of the wafers of the C-brick are relatively smaller than those of the S-brick wafers. This indicates that the dislocation cluster ratio of the C-brick wafers is notably lower than that of the S-brick wafers. Based on Fig. 3, the dislocation

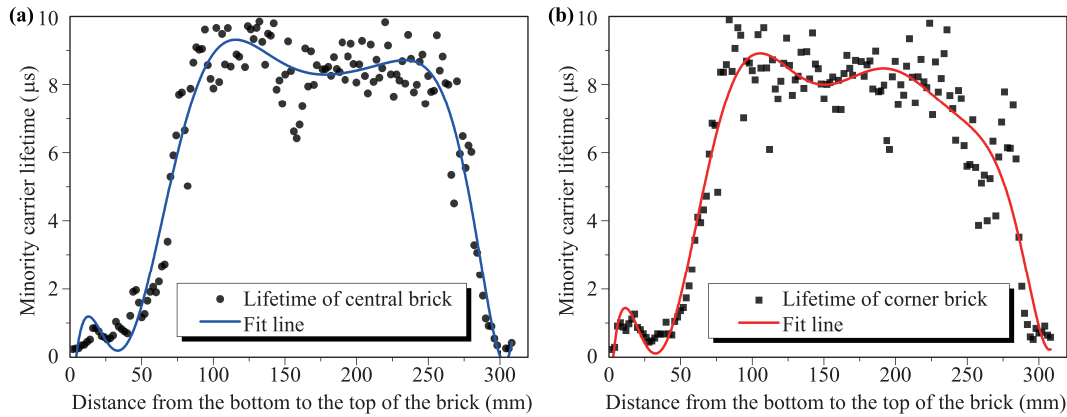

Fig. 2 The distribution of the minority carrier lifetime in the **(a)** central brick and **(b)** side brick.

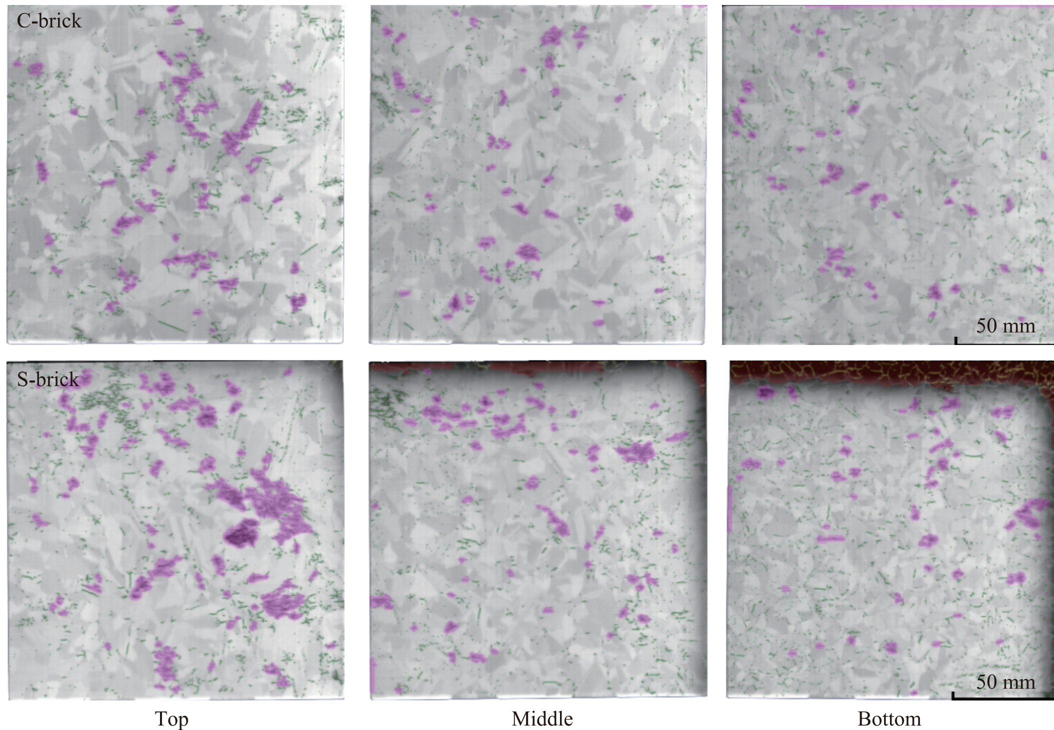

Fig. 3 PL maps of the wafers at different heights for the central and side bricks.

cluster distribution is random and its ratio is higher at the top of both bricks than in the middle and bottom. The brown region decreases from the bottom to the top, which agrees well with the distribution of the red region of the ingot shown in Fig. 1.

Dislocations can cause electronic states in the forbidden band of Si and act as heavy recombination centers. The average values of dislocation clusters and grain boundaries are displayed in Figs. 4(a) and (b). The average dislocation cluster ratio decreases from the top to the bottom, while the low-lifetime region increases. Therefore, dislocations do not cause the lifetime distribution of the periphery edge. In addition, the average grain boundary ratio of the wafers in the middle position is lower than that in other positions. The placement of the seed crystals in the initial period of grain growth leads to disordered grain orientation. As effect of seeds in the medium period, small grains become larger and one or more twin structures ($\sum 3$ boundaries) are produced [16–18]. Although the dislocations begin to propagate

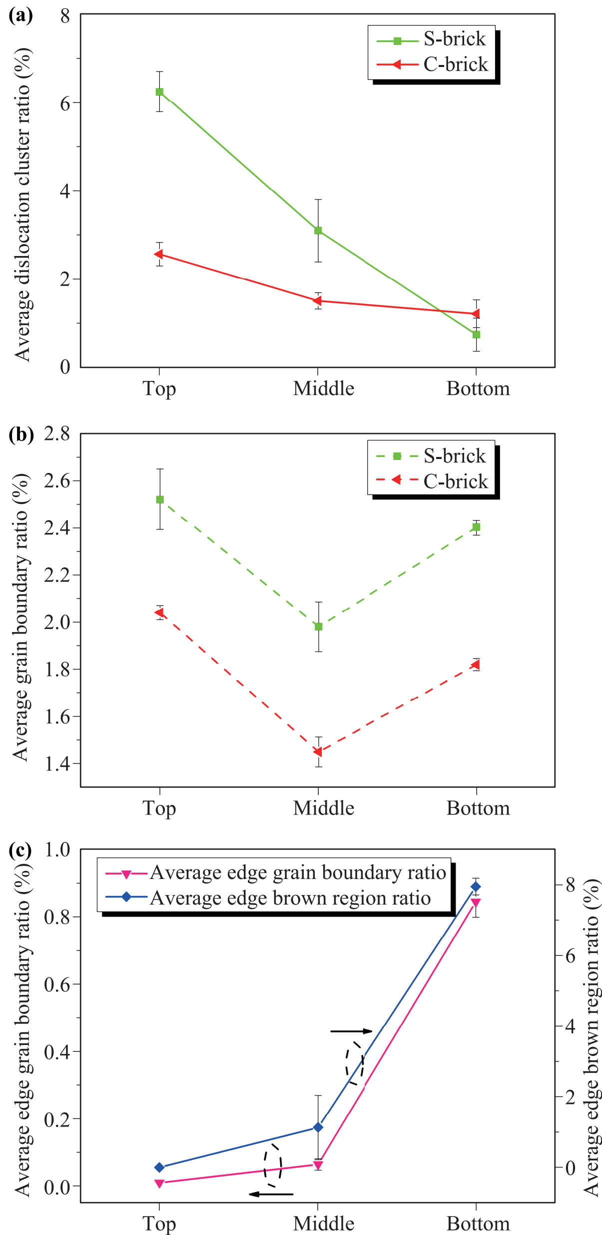

Fig. 4 The distribution of **(a)** average dislocation and **(b)** boundary ratios of the wafers at different heights for the central and side bricks and **(c)** edge boundary ratio and brown edge area of the side brick.

and multiply as mc-Si is growing, the dislocation movement to boundaries becomes easier, which might lower the possibility of dislocation clusters. Therefore, the average dislocation cluster ratio increases slightly and the average gain boundary ratio decreases in the medium period. The segregation of directional solidification in the later period leads to many impurities assembling in the top part of the mc-Si ingot. This induces dislocation propagation and plays a role for nucleation centers, which lead to of the increase of dislocation clusters and grain boundaries. The average grain boundary ratio of 0.84% corresponds to the low-lifetime region (7.94%) in the bottom of the S-brick. The average grain boundary ratio of 1.56% corresponds to other regions (92.06%). Therefore, the grain boundary per unit area of the low-lifetime edge is more than 5.5 times that of the high-lifetime region. The inhomogeneous boundary distribution results in small grain areas at the edge and consequently in a periphery edge exhibiting a lower minority carrier lifetime.

3.3 Impurities

Square silicon chips from the bottom position were used for impurity concentration measurements, as shown in Table 1 and Fig. 5. Iron impurities were considered to be the cause of the red periphery zone in multicrystalline ingots because of their high solubility and diffusivity [19]. Compared with the Fe concentration maps of the C-brick, the Fe concentration maps of the S-brick displays an inhomogeneous distribution [Figs. 5(a) and (b)]. The average iron concentration of the low-lifetime edge of the S-brick is 1.58×10^{12} cm^{-3}, which is larger than that of the high-lifetime region (1.39×10^{12} cm^{-3}), corresponding to an increase of 0.19×10^{12} cm^{-3}. Therefore, iron impurities are relevant for the low-lifetime region of the S-brick.

The FTIR absorption spectrum was processed using Gaussian curve fitting. The concentration of carbon and oxygen impurities in 16 samples was calculated after the fitted baseline was subtracted. The concentration of carbon impurities was estimated [Figs. 5(c) and (d)]. A sample with a carbon concentration higher than 1.20×10^{18} was found. The oxygen concentration of S-brick edge samples is on average higher than that of high-lifetime regions, as shown in Fig. 5(e). This phenomenon has been discussed in our preliminary work [15]. Based on Fig. 5(f), the oxygen distribution of most samples is homogeneous, ranging between 8.50×10^{17} and 9.00×10^{17}. The concentrations of substitutional carbon and inter-

Table 1 The average impurity concentration of the edge and high-lifetime regions of the central and side bricks.

	Sample	Fe (cm^{-3})	C (cm^{-3})	O (cm^{-3})
C-brick	Edge (0 mm)	1.46×10^{12}	6.58×10^{17}	8.23×10^{17}
	High lifetime region (120 mm)	1.42×10^{12}	6.59×10^{17}	7.76×10^{17}
S-brick	Edge (0 mm)	1.58×10^{12}	7.78×10^{17}	7.23×10^{17}
	High lifetime region (120 mm)	1.39×10^{12}	6.19×10^{17}	8.90×10^{17}

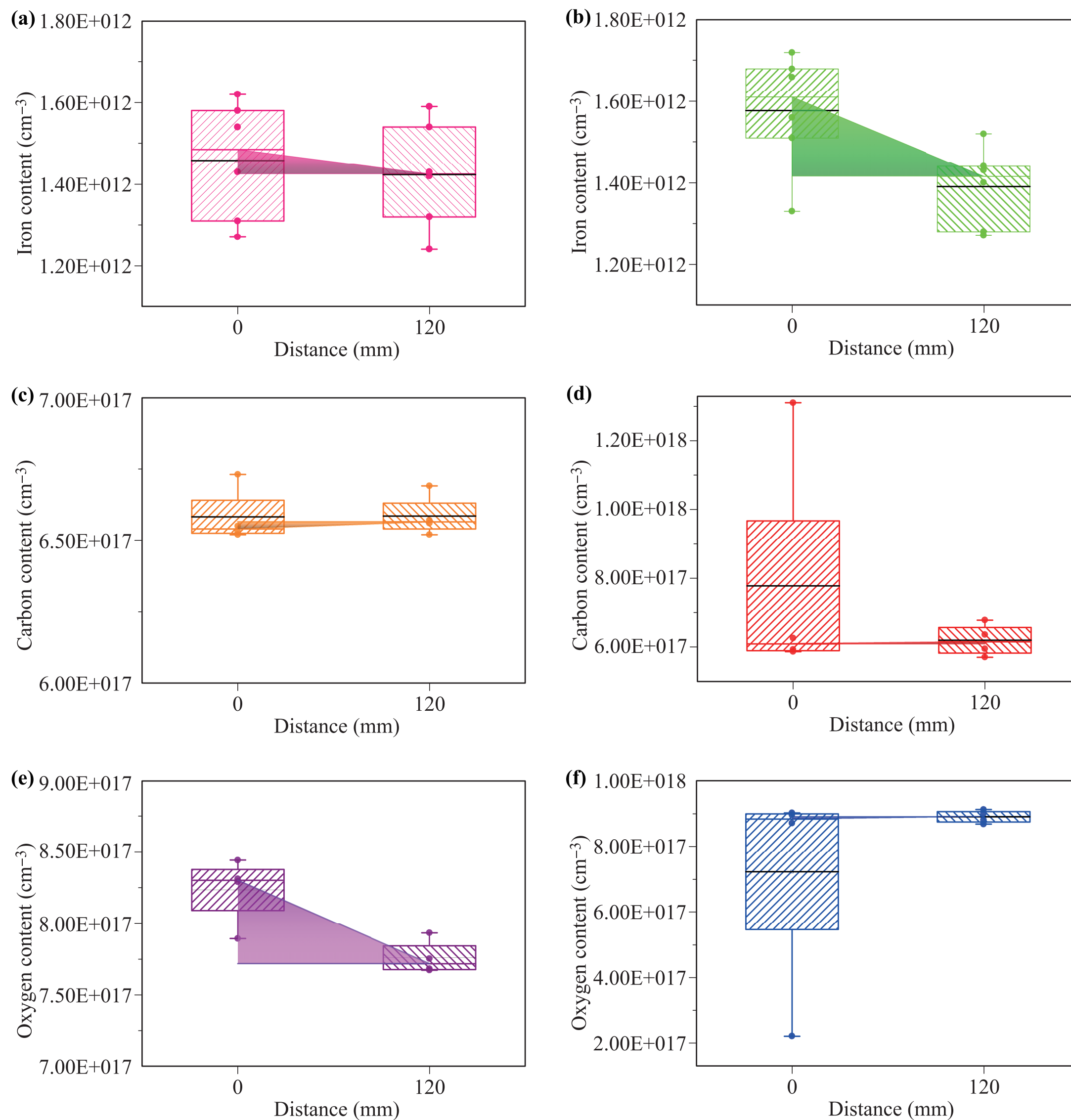

Fig. 5 Iron, carbon, and oxygen concentration of the edge and high-lifetime regions of the central and side bricks based on FTIR spectroscopy.

stitial oxygen are mainly at a reasonable level; the concentrations at the edge did not notably differ from that of the center. Therefore, C and O impurities are not the cause of the low periphery edge lifetime.

3.4 Improvement of crystalline growth

Based on the experiment and discussion of the effect of defects and impurities on the periphery edge lifetime, it can be concluded that the Fe impurities and small grain region of the S-brick lower the ingot quality. It is difficult to completely remove Fe impurities using quartz crucibles for industrial mc-Si ingot production. However, controlling the impurities, including C and O, is still a suitable way to improve the mc-Si quality [20, 21]. The grain growth affected by seed crystals competes with the crystals nucleated in the side crucible of the S-brick, which results in higher boundary density at the localized edge compared with other regions, leading to lower minority carrier diffusion. There is no doubt that seed preservation plays an important role in the generation of low-lifetime periphery edges; thus, the surface of the seed region should be as flat as possible during crystal growth.

There are two ways to further improve the quality of the mc-Si ingot: Firstly, lowering the possibility of further contamination with impurities (carbon and oxygen) by optimizing the argon flow; and secondly, flattening

the surface of seed crystals by adjusting the temperature distribution. Based on our casting experiment [8], the surface of the seed region is flatter than before. In addition, our experiment also confirms that the ingot quality improved (0.13 μs) and on average 2.14% minority carrier lifetime and effective minority carrier lifetime were gained.

4 Conclusion

The effect of possible impurities and defects on the generation of low-lifetime periphery edges in a high-performance industrial mc-Si ingot was analyzed. The average iron concentration of the low-lifetime edge of the S-brick is $\sim 0.19\times10^{12}$ cm^{-3} larger than that of the high-lifetime region. At the bottom of the high-performance mc-Si ingot, the boundary per unit area of the low-lifetime edge is more than 5.5 times that of the high-lifetime region. It has been demonstrated that the iron impurity contamination from crucibles and high boundary density at the localized edge cause the low minority carrier lifetime of the periphery edge. Seed preservation has been proven to be relevant for the low-lifetime region of the side brick and a flatter seed region is beneficial for growing a high-quality silicon ingot. Based on controlling the impurity contamination and improving the grain size distribution, improvements were achieved; these measures can be applied to manufacture industrial multicrystalline ingots for solar cells.

Acknowledgements This work was financially supported by Guangzhou Science and Technology Department (Grant No. 2014Y2-00221). We are also grateful to Ms. Lei Zeng from the Shangdong DAHAI New Energy CO., Ltd., for her help with the mc-Si casting experiments.

References

1. F. Q. Huang, C. Y. Yang, and D. Y. Wan, Advanced solar materials for thin-film photovoltaic cells, *Front. Phys.* 6(2), 177 (2011)
2. N. P. Dasgupta and P. Yang, Semiconductor nanowires for photovoltaic and photoelectrochemical energy conversion, *Front. Phys.* 9(3), 289 (2014)
3. W. L. Chen, G. S. Shen, Z. Wu, Z. Li, and R. J. Hong, Optimizing transparent conductive Al-doped ZnO thin films for SiN_x free crystalline Si solar cells, *J. Mater. Sci. Mater. Electron.* 27(7), 7566 (2016)
4. J. D. Li, G. S. Shen, W. L. Chen, Z. Li, and R. J. Hong, Preparation of SiN_x multilayer films by mid-frequency magnetron sputtering for crystalline silicon solar cells, *Mater. Sci. Semicond. Process.* 59, 40 (2017)
5. Z. L. Wang, W. H. Xie, and Y. H. Zhao, Tunable band structure and effective mass of disordered chalcopyrite, *Front. Phys.* 12(1), 127103 (2017)
6. Z. Y. Wu, G. X. Zhong, Z. Y. Zhang, X. C. Zhou, Z. X. Wang, and X. M. Huang, Optimization of the high-performance multi-crystalline silicon solidification process by insulation partition design using transient global simulations, *J. Cryst. Growth* 426, 110 (2015)
7. Y. M. Yang, A. Yu, B. Hsu, W. C. Hsu, A. Yang, and C. W. Lan, Development of high-performance multicrystalline silicon for photovoltaic industry, *Prog. Photovolt. Res. Appl.* 23(3), 340 (2015)
8. J. D. Li, Y. F. Chen, and R. J. Hong, Modeling and optimization of the feedstock melting for industrial photovoltaic multi-crystalline silicon ingot, *Sol. Energy* 139, 108 (2016)
9. T. T. Jiang, X. G. Yu, L. Wang, X. Gu, and D. R. Yang, On the low carrier lifetime edge zone in multicrystalline silicon ingots, *J. Appl. Phys.* 115(1), 012007 (2014)
10. A. A. Istratov, T. Buonassisi, R. J. McDonald, A. R. Smith, R. Schindler, J. A. Rand, J. P. Kalejs, and E. R. Weber, Metal content of multicrystalline silicon for solar cells and its impact on minority carrier diffusion length, *J. Appl. Phys.* 94(10), 6552 (2003)
11. D. P. Fenning, J. Hofstetter, M. I. Bertoni, S. Hudelson, M. Rinio, J. F. Lelievre, B. Lai, C. del Canizo, and T. Buonassisi, Iron distribution in silicon after solar cell processing: Synchrotron analysis and predictive modeling, *Appl. Phys. Lett.* 98(16), 162103 (2011)
12. A. A. Istratov, H. Hieslmair, and E. R. Weber, Iron contamination in silicon technology, *Appl. Phys. A* 70(5), 489 (2000)
13. M. Trempa, C. Reimann, J. Friedrich, G. Müller, L. Sylla, A. Krause, and T. Richter, Investigation of iron contamination of seed crystals and its impact on lifetime distribution in Quasimono silicon ingots, *J. Cryst. Growth* 429, 56 (2015)
14. V. Osinniy, P. Bomholt, A. Nylandsted Larsen, E. Enebakk, A. K. Søiland, R. Tronstad, and Y. Safir, Factors limiting minority carrier lifetime in solar grade silicon produced by the metallurgical route, *Sol. Energy Mater. Sol. Cells* 95(2), 564 (2011)
15. X. X. Liu, G. H. Yan, and R. J. Hong, Generation mechanism of inhomogeneous minority carrier lifetime distribution in high quality mc-Si wafers and the impacts on electrical performance of wafers and solar cells, *J. Mater. Sci. Technol.* 31(11), 1094 (2015)
16. H. Y. Wang, N. Usami, K. Fujiwara, K. Kutsukake, and K. Nakajima, Microstructures of Si multicrystals and their impact on minority carrier diffusion length, *Acta Mater.* 57(11), 3268 (2009)
17. X. H. Tang, L. A. Francis, L. F. Gong, F. Z. Wang, J. P. Raskin, D. Flandre, S. Zhang, D. You, L. Wu, and B. Dai, Characterization of high-efficiency multicrystalline silicon in industrial production, *Sol. Energy Mater. Sol. Cells* 117(10), 225 (2013)

18. K. M. Yeh, C. K. Hseih, W. C. Hsu, and C. W. Lan, High-quality multi-crystalline silicon growth for solar cells by grain-controlled directional solidification, *Prog. Photovolt. Res. Appl.* 18(4), 265 (2010)

19. D. Macdonald, A. Cuevas, A. Kinomura, Y. Nakano, and L. J. Geerligs, Transition-metal profiles in a multicrystalline silicon ingot, *J. Appl. Phys.* 97(3), 033523 (2005)

20. D. R. Yang, L. B. Lia, X. Y. Ma, R. X. Fan, D. L. Que, and H. J. Moeller, Oxygen-related centers in multicrystalline silicon, *Sol. Energy Mater. Sol. Cells* 62(1–2), 37 (2000)

21. L. J. Liu, S. Nakano, and K. Kakimoto, Carbon concentration and particle precipitation during directional solidification of multicrystalline silicon for solar cells, *J. Cryst. Growth* 310(7–9), 2192 (2008)